Chem Soc Rev

Cite this: *Chem. Soc. Rev.*, 2012, **41**, 7994–8008

www.rsc.org/csr

TUTORIAL REVIEW

Bimetallic catalysts for hydrogen generation†

Zhehao Wei,[a] Junming Sun,*[a] Yan Li,[a] Abhaya K. Datye[c] and Yong Wang*[ab]

Received 3rd June 2012
DOI: 10.1039/c2cs35201j

Research interest in bimetallic catalysts is mainly due to their tunable chemical/physical properties by a number of parameters like composition and morphostructure. In catalysis, numerous bimetallic catalysts have been shown to exhibit unique properties which are distinct from those of their monometallic counterparts. To meet the growing energy demand while mitigating the environmental concerns, numerous endeavors have been made to seek green and sustainable energy resources, among which hydrogen has been identified as the most promising one with bimetallic catalysts playing important roles. This tutorial review intends to summarize recent progress in bimetallic catalysts for hydrogen production, specifically focusing on that of reforming technologies as well as the relevant processes like water-gas shift (WGS) and CO preferential oxidation (PROX), and emphasizing on the fundamental understanding of the nature of catalytic sites responsible for generating high purity hydrogen and minimizing carbon monoxide formation. Meanwhile, some important synthesis and characterization methods of bimetallic catalysts developed so far are also summarized.

1. Introduction

Materials, when their dimensions fall in the range of a few nanometers, exhibit distinct surface chemical/physical properties from their individual atoms or the bulky matter.[1] In catalysis, unique catalytic performances have been observed on these so-called nanocatalysts. Bimetallic catalysts, composed of two metal elements in either alloy or intermetallic form, often emerge as materials of a new category with catalytic properties different from monometallic catalysts,

[a] *The Gene & Linda Voiland School of Chemical Engineering and Bioengineering, Washington State University, Pullman, WA 99164, USA. E-mail: Junming.sun@wsu.edu*
[b] *Institute for Integrated Catalysis, Pacific Northwest National Laboratory, Richland, WA 99352, USA. E-mail: Yong.Wang@pnnl.gov*
[c] *Department of Chemical and Nuclear Engineering and Center for Microengineered Materials, University of New Mexico, Albuquerque, New Mexico 87131, USA*
† Part of the bimetallic nanocatalysts themed issue.

Zhehao Wei

Zhehao Wei received his double BS degrees in 2008, one in Chemistry from Nankai University and the other in Chemical Engineering from Tianjin University. Two years later, he obtained his MS degree in Chemical Engineering from Tianjin University under the supervision of Prof. Changjun Liu. He is currently pursuing his PhD in Chemical Engineering at Washington State University under the supervision of Prof. Yong Wang. His research focuses on in situ characterization of heterogeneous catalysts and biomass conversion for clean energy production.

Junming Sun

Junming Sun is a research assistant professor in Prof. Yong Wang's group in the Gene & Linda Voiland School of Chemical Engineering and Bioengineering, Washington State University, USA. He received his PhD from Dalian Institute of Chemical Physics of Chinese Academy of Science in 2007 (supervised by Prof. Xinhe Bao), after which he worked as a postdoc researcher with Prof. Bruce C. Gates at University of California, Davis (2007–2008) and with Prof. Yong Wang at Pacific Northwest National Laboratory, USA (2008–2011). His current research interests include catalytic biomass conversion, bio-oil upgrading, hydrogen and fuel production, and nano-catalysis.

depending on the composition and size/morphology. Initial studies on bimetallic catalysts by Sinfelt date back to the early 1960s,[2] which have since stimulated intensive research interests worldwide. The unremitting endeavor in this particular field, especially in conjunction with the development of nanotechnology for energy generation,[3] has provided some insight into the catalytic behavior in terms of the catalyst structure–property relationship. Scientific research has proved that bimetallic catalysts possess unique properties strongly associated with their intrinsic electronic/geometric structures.[4] It is noteworthy that these novel materials generally exhibit enhanced catalytic performances over traditional monometallic ones.[1,5] Various catalyst characterization methods have been developed and employed to unravel the riddle in bimetallic catalysis. Fundamental studies on single crystal/model bimetallic catalysts and calculations by density functional theory (DFT) also provide supportive evidence to their catalytic behavior[6] for applications including catalytic hydrogen production.

Hydrogen has a wide range of applications in our lives nowadays, primarily in chemical and refining industries for the synthesis of ammonia and methanol as well as the control of sulfur and aromatic components in liquid fuels. Recent development of proton exchange membrane fuel cell (PEMFC) has opened a new era for highly efficient utilization of hydrogen,[7] in which hydrogen and oxygen are converted to generate electricity with water being a side product. Currently, hydrogen is mainly generated from steam methane reforming (SMR), which accounts for 95% hydrogen produced in the US.[8] Hydrogen can also be produced from other resources *via* processes like biomass conversion, ammonia cracking and water splitting,[7,8] among which catalysis inevitably plays key roles.[9]

To date, despite the intensive literature reviews on catalytic hydrogen production,[7,9,10] the need for a detailed review on bimetallic catalysts for hydrogen generation as well as the down-stream purification processes remains. In this tutorial review, the importance and recent development of bimetallic catalysts are introduced along with their applications in catalytic hydrogen production. Specifically, we focus on the recent development with respect to supported bimetallic catalysts for high-purity hydrogen production from reforming techniques as well as the relevant processes such as water-gas shift (WGS) and CO preferential oxidation (PROX). Meanwhile, some important synthesis and characterization methods of bimetallic catalysts developed so far are also summarized.

Yan Li

Yan Li earned her BS and MS degrees in Chemical Engineering from Tianjin University in 2008 and 2010, respectively. Her MS research involved nickel catalyst development for reforming of methane under the supervision of Prof. Chang-jun Liu. She is currently pursuing her PhD degree at Washington State University on the fundamental research of metal oxide catalysts for selective oxidation reactions.

2. Bimetallic catalyst synthesis, treatment/activation and characterization

2.1 Synthesis

Preparation method usually affects the properties of bimetallic catalysts and consequently their catalytic performances.[11,12] Various methods have been reported for bimetallic catalyst synthesis, including vapor deposition, impregnation, co-precipitation (CP), deposition-precipitation (DP), liquid-phase synthesis, and aerosol-derived approach, which are briefly summarized in Table 1.

2.1.1 Vapor deposition. Vapor deposition is one of the most important sample preparation methods in surface science,

Abhaya K. Datye

Abhaya Datye has been on the faculty at the University of New Mexico since 1984. He is also the director of the graduate interdisciplinary program in Nanoscience and Microsystems. He serves as Director of the Center for Microengineered Materials at UNM. His research interests are the synthesis of biorenewable chemicals, fundamental studies of catalyst sintering, alcohol reforming into H_2 and synthesis of novel nanostructured heterogeneous catalysts. He leads the NSF Partnership for international research and education on conversion of biomass derived reactants into fuels and chemicals (a collaboration between faculty and researchers in the US, Denmark, Germany, Netherlands and Finland).

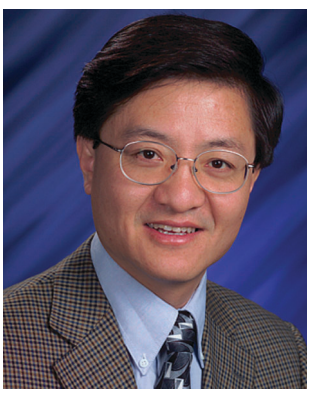

Yong Wang

Yong Wang joined Pacific Northwest National Laboratory (PNNL), USA, in 1994 and was promoted to a Laboratory Fellow in 2005. In 2009, he assumed a joint position at Washington State University (WSU) and PNNL. In this unique position, he continues to be a Laboratory Fellow/Associated Director of Institute for Integrated Catalysis at PNNL and is the Voiland Distinguished Professor in Chemical Engineering at WSU. His research interests include the development of novel catalytic materials and reaction engineering for the conversion of fossil and biomass feedstocks to fuels and chemicals.

Table 1 Bimetallic catalyst synthesis methods

Name of method (abbr.)	Key features	Advantages	Disadvantages	Example and Ref.
Vapor deposition	Model catalyst preparation for surface science studies	Flexible control of the bimetallic surface and overlayers	UHV conditions and preparation apparatus are required	Ni/Pt(111)[6]
Incipient wetness impregnation (IWI)	Most widely used preparation method	Simple preparation	Poor control of particle size and element distribution	Pt–Ni/Al_2O_3,[12] Pt–Co/YSZ,[14] Pt–Re/C[17]
Co-precipitation (CP)	Simultaneous precipitation of the two metals can be achieved	Easy control of particle size and composition	Accurate control of co-precipitation and impurity (by precipitant) removal steps are required	Pd/ZnO[21]
Deposition–precipitation (DP)	Widely used in preparation of supported metal catalysts, such as Au-based ones	Applicable to high metal loading with a small particle size and narrow distribution; maximum metal–support interaction	Accurate control of precipitation and impurity (by precipitant) removal steps are required; metal–support interaction is required	Au–Ru/Fe_2O_3, Au–Cu/TiO_2[63]
Liquid-phase synthesis	Colloidal synthesis of bimetallic NPs	Easy and flexible control of particle size, shape, uniformity of composition	Precise control of synthesis parameters and removal of impurities introduced by reducing agents/surfactant is required	M@Pt core–shell NP,[23] Pd–Pt alloy nanocage[24]
Aerosol-derived approach	Unsupported catalyst with sufficiently high surface area for reactivity testing under industrially relevant conditions[25]	Homogeneous composition, uniform particle size	Large particle size; special apparatus for catalyst preparation is needed	PdZn alloy powder[25]

and mainly includes physical vapor deposition (PVD), chemical vapor deposition (CVD) and electrochemical deposition (ECD). For bimetallic model catalyst preparation, vapor deposition is conducted by applying suitable parameters, such as choice of metal source(s) and appropriate substrate, rate of metal vapor generation, deposition duration, substrate temperature, and gas atmosphere or ultra-high vacuum (UHV).[6]

2.1.2 Impregnation. Due to its easy operation and inexpensiveness, impregnation has been widely used for catalyst synthesis. Wetness impregnation (WI) requires the support to be dipped into a precursor solution to achieve the loading of active components. Incipient wetness impregnation (IWI) limits the volume of the precursor solution to just match the pore volume of the catalyst support to maximize the loading of active components in the pore matrix of the catalyst support. The concentration of the precursor solution can be adjusted to control the loading amounts of the active phase. For bimetallic catalysts requiring more than one metal precursor, either co-impregnation (CI)[12–14] or sequential impregnation (SI)[12,15–18] can be used. The impregnation method may result in broad distribution of metal particle size and uneven element composition due to preferential adsorption of metal precursors on the support or enrichment of precursors during drying, which complicates the investigation of catalyst structure-properties.[19,20]

2.1.3 CP and DP. Compared with impregnation, CP has a better control of particle size and distribution of elements in bimetallic catalysts. It is usually carried out by adding a precipitant into a solution consisting of at least two metal salt precursors serving as the bimetallic sources.[21] The key objective of this method is to achieve simultaneous precipitation of different metals by controlling the processing conditions including pH. Ammonium hydroxide is generally used as the precipitant to avoid extra steps for eliminating impurity ions. Appropriate thermal treatment is sometimes used to improve the crystallization of precipitates.

DP is another method that involves a more precise control of the precipitation process to prepare supported catalysts.[22] Typically, support is first premixed with a soluble metal precursor. Then the metal precursor can be converted into another form of lower solubility and specifically deposited onto the support surface. This conversion can be done by changing the pH of the solution, the valence state of the metal precursor, or the concentration of a complexing agent. Interaction between the metal precursor and the support is essential to favor the precipitation of the metal precursor onto the support surface over that in solution, possibly due to enrichment of precipitate or precipitant on the support surface. One key is to add the precipitant gradually with constant stirring to avoid abrupt rise of local concentration and thus precipitation in solution. With this dedicated control, highly dispersed metal (oxide, sulfide, *etc.*) catalysts can be prepared even at high loadings. In bimetallic catalyst preparation, an aqueous solution containing two metal precursors is usually used, and a more dedicated process is required to ensure simultaneous precipitation of two distinct metals.

2.1.4 Liquid-phase synthesis. Liquid-phase synthesis involves a chemical reaction by which the reactant can be converted into the target product in a confined space (*e.g.*, micelle). The major advantages of this method are its relative simpleness and flexibility in controlling the particle size, uniformity of composition and even morphostructure of the obtained catalysts. For bimetallic nanoparticle (NP) synthesis, one needs to control the thermodynamics and kinetics of nucleation and growth of two distinct metals. The details regarding the solution-based synthesis have been well summarized

and reviewed by Wang and Li.[5] Co-reduction[23] and galvanic replacement[24] are two popular methods in colloidal synthesis to prepare bimetallic particles with unique structures.

2.1.5 Aerosol-derived approach. In the aerosol-derived wet-chemistry synthesis, liquid-form metal precursor is first ultrasonically atomized to very small and uniform droplets. Then the droplets pass through a high-temperature zone under a given atmosphere, going through a fast drying and decomposition/oxidation process and forming oxide particles collected on a filter at the outlet of the furnace. When a solution of two different metal precursors is used, bimetallic catalysts can be synthesized. For instance, the Datye group successfully synthesized an unsupported PdZn catalyst with homogeneous composition.[25] Apart from the uniform particle size with controllable composition, another obvious advantage of this synthesis approach is synthesizing unsupported catalysts with sufficiently high metal surface area for catalysis study without the interference of support. However, it is difficult to synthesize catalytic materials with a particle size as small as a few nanometers using this approach.

2.2 Treatment/activation

Traditional and typical catalyst treatment and activation can be indiscriminately applied to bimetallic catalysts. These prior-to-reaction treatment processes usually consist of drying, calcination and reduction steps. The basic functions of these steps can be simplified as: drying allows the metal precursors to attach to the pore walls while vaporizing solvents; calcination brings about the decomposition of metal precursors forming metal oxides while eliminating volatile species in metal precursors; reduction leads to the formation of the catalytic active phase (core–shell, heterostructure, or intermetallic/alloy), which is generally regarded as the most important catalyst activation step. However, recent research findings suggest that, in some cases, the reduction step is not necessary since catalysts can be activated *in situ* under reaction conditions.[11,26] For bimetallic catalysts prepared in a sequential (or multi-step) manner, an intermediate treatment is usually needed before loading a second metal precursor.[12,18]

2.3 Characterization

Characterization of bimetallic catalyst structure is the key to uncover their intrinsic structure–property relationship. Recent advancement in characterizations, particularly the *in situ* techniques, have proven to be the powerful and insightful tools to unravel the relationship between catalyst structures with their catalytic performances.[27] Herein, we also briefly summarize some important characterization tools developed so far for structure identification of bimetallic catalysts.

2.3.1 X-ray diffraction (XRD). XRD has been broadly used for phase identification and crystal structure determination in material science. This technique is particularly suitable for bulk structure characterization of bimetallic catalysts such as alloy formation between Pd–Zn,[11,21,25,28–32] Ni–Sn[33] and Au–Cu.[34] For example, Chin *et al.* found that the XRD pattern (Fig. 1) of Pd/ZnO catalyst reduced at temperatures

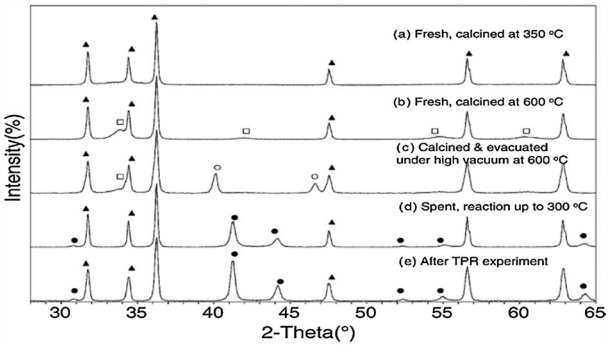

Fig. 1 XRD patterns of Pd/ZnO (diffraction peak denotation: ▲ ZnO, □ PdO, ○ Pd, ● PdZn).[29] Reproduced by permission of Elsevier.

higher than 300 °C exhibited diffraction peaks other than those assigned to Pd or ZnO, suggesting the formation of a new phase (PdZn alloy) with different lattice distances.[29] However, XRD is limited to characterizing crystalline materials. Disordered, amorphous material and nano-crystalline (< 2 nm in size) are beyond the detection limit of XRD and rely on other characterization techniques such as electron microscopy and X-ray absorption spectroscopy (XAS) to be discussed below.

2.3.2 Electron microscope (EM) and accessories. In contrast to XRD, electron microscopy is more suitable for identifying local structural information of catalysts. In particular, the high-resolution electron microscopes (HREMs), such as aberration-corrected high-resolution transmission electron microscope (HRTEM) and high angle annular dark field scanning transmission electron microscope (HAADF-STEM), are capable of imaging at atomic resolution, together with the accessories such as energy-dispersive X-ray spectroscopy (EDX), electron energy-loss spectroscopy (EELS) and selected-area electron diffraction (SAED). With respect to bimetallic catalysts, evidence on particle morphology, dispersion, crystallinity and crystalline structure, as well as the surface composition and homogeneity can be characterized.[21,25,29,31,32,35] For example, Zhang *et al.* synthesized Pd–Pt alloy nanocages and characterized their morphology, structure and composition using EMs (Fig. 2).[24]

2.3.3 Scanning tunneling microscopy (STM). Based on the quantum tunneling concept, STM was invented by Binnig and Rohrer in 1981 and has since been advanced for material studies at atomic level. With a very sharp tip where only one atom serves as the apex, STM is capable of providing surface information of a given material by recording the tunneling current with respect to the tip position. For catalyst studies, STM is especially helpful to reveal the mechanistic aspect of catalytic processes. Technical advancement has expanded the application of STM from UHV to atmospheric and even higher-pressure environment,[36] making *in situ* characterization possible.[37,38] Using STM in bimetallic catalyst studies has received vast attention.[39]

2.3.4 Temperature-programmed reduction (TPR). A number of temperature-programmed techniques have been utilized to

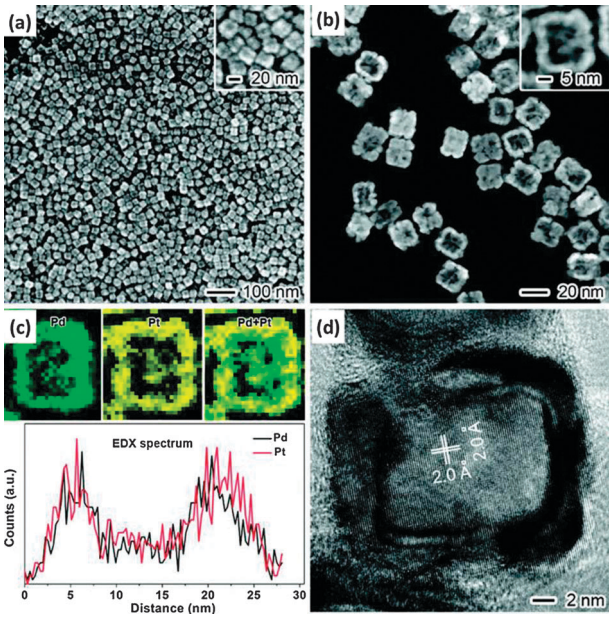

Fig. 2 EM characterizations of the Pd–Pt alloy nanocages: (a) SEM image, (b) HAADF-STEM image, (c) EDX mapping and line-scan profile, and (d) HRTEM image.[24] Reproduced by permission of American Chemical Society.

study the surface chemistry and redox properties of catalysts. Among these, H_2-TPR has proven to be a powerful tool to provide quantitative information on the reducibility of surface metal oxide as well as the metal–metal interactions in bimetallic catalysts, or the so-called synergistic effect.[12–13,40–44] For instance, Strohm *et al.* performed a set of TPR experiments to examine the promotion effect of Ni to Rh/CeO_2–Al_2O_3 catalyst.[13] As can be seen in Fig. 3, the TPR profile clearly shows that the RhO_x reduction peaks shift towards high temperatures as the Ni loading increases, implying more intimate interaction between Rh and Ni at higher Ni loadings and most Rh is associated with Ni at > 5% Ni loadings.

2.3.5 X-ray photoelectron spectroscopy (XPS). XPS is a spectroscopic technique examining elemental composition, oxidation state, chemical environment, and electronic structure of the elements on material surfaces. As for bimetallic catalysts, XPS can provide the information related to electronic properties, including the electron transfer between two metals, which are believed to play critical roles in modifying the catalyst properties.[13,18,45–47] For example, an *in situ* treated Pt–Re/C bimetallic catalyst followed by XPS characterization (Fig. 4a) by Zhang *et al.* showed that the reduced catalyst involved positively charged Pt of which the extent of electron-deficiency increased with the Re amount, suggesting the Pt–Re alloy structure and electron transfer from Pt to Re.[18] Most importantly, the divergence of operation conditions between UHV XPS and realistic catalytic reactions has promoted the advancement of the XPS technique. Ambient-pressure XPS (APXPS) has been recently reported[48] to be possible for *in situ* studies of catalysts at realistic reaction atmosphere.[49]

2.3.6 Fourier transform infrared spectroscopy (FTIR). FTIR is a surface sensitive characterization tool for identifying surface functional groups and measuring catalyst surface structure. *In situ* diffuse reflectance infrared Fourier transform spectroscopy (DRIFTS)[45] and attenuated total reflectance infrared spectroscopy (ATR-IRS)[50] have been extensively used to identify intermediates/products formed on the catalyst surface as well as to understand the catalyst surface evolution under the reaction conditions. Despite the recent development in fast-data acquisition, dynamic IR studies of surface reactions at a time scale (*e.g.*, femtosecond and picosecond) of evolution of reaction intermediates are still challenging. IR analysis of stable adsorbates remains a common and useful method to probe the surface chemistry of catalysts.

Characterizing bimetallic catalysts with FTIR takes advantage of the interaction of probe molecules (*e.g.*, CO, NO, *etc.*) and the catalyst surface active sites.[12,16,18,20,23,35,45,51] Using CO-DRIFTS, Li *et al.*[20] found that Al_2O_3 supported Pt–Ni

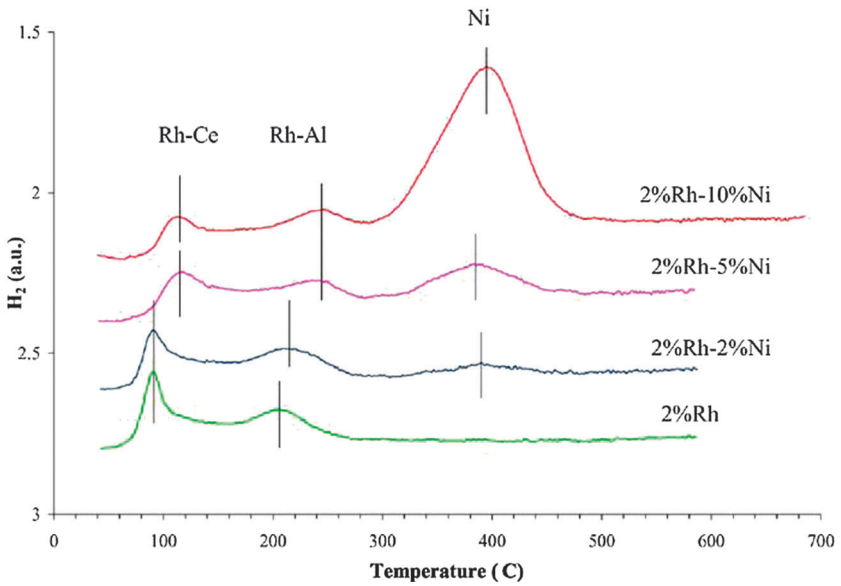

Fig. 3 TPR profiles of Rh–Ni/CeAl catalysts with different Ni loadings.[13] Reproduced by permission of Elsevier.

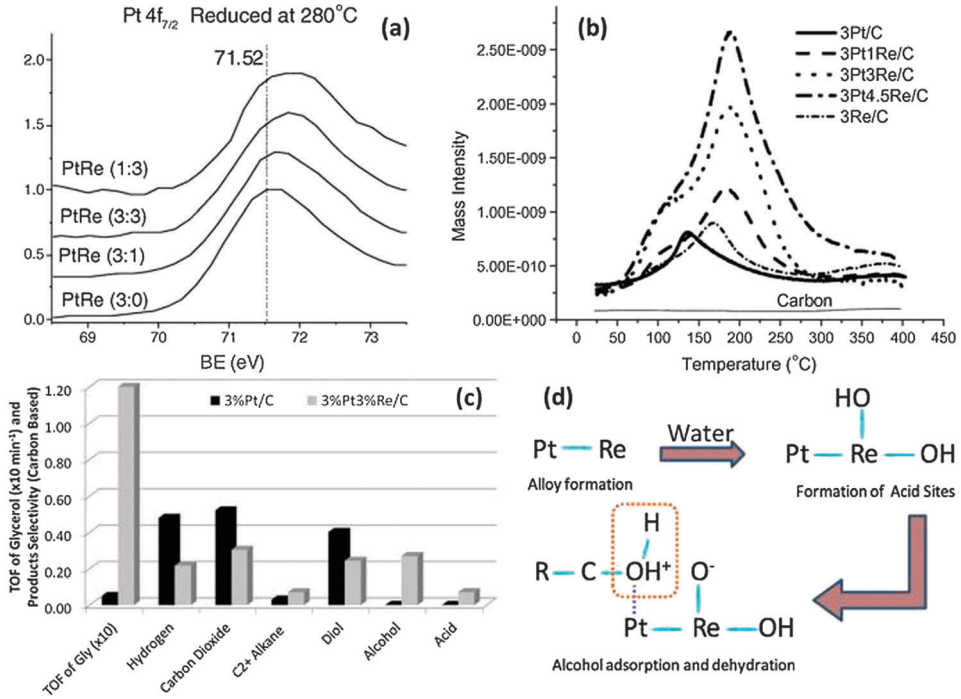

Fig. 4 (a) XPS results (Pt $4f_{7/2}$) of reduced Pt–Re/C catalysts with different Pt/Re ratios, (b) NH_3-TPD of Pt–Re/C with varying Pt/Re ratio, (c) TOF and selectivity (carbon based) for APR of 10% glycerol over 3%Pt/C and 3% Pt–3% Re/C at 225 °C and 2.9 MPa, (d) bimetallic Pt–Re catalyst structure evolution upon exposure to water and alcohol.[18] Reproduced by permission of Elsevier.

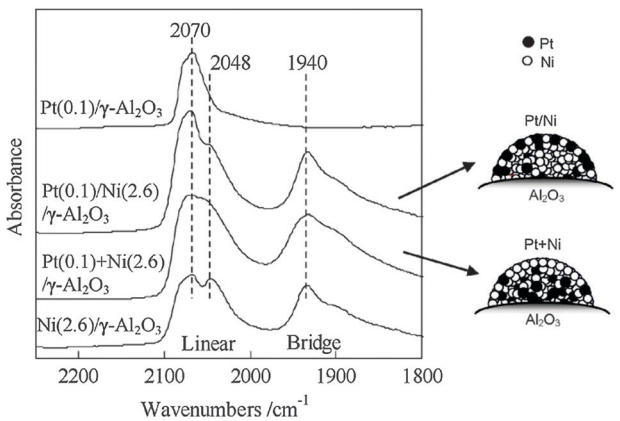

Fig. 5 FTIR spectra of CO adsorption and structural model of Pt–Ni bimetallic particles.[20] Reproduced by permission of Elsevier.

bimetallic catalysts prepared using co-impregnation resulted in maximum surface Ni exposure which was similar to the Ni alone catalyst (Fig. 5), while sequential impregnation led to surface Pt segregation.

2.3.7 XAS. The growing interest in using XAS for catalytic material characterization is evidenced by the rapidly increasing publications involving XAS utilization. To date, the major benefit of XAS to the catalysis field seems to be associated with the structure analysis in two featured regions of a spectrum, namely, X-ray absorption near-edge structure (XANES) and extended X-ray absorption fine structure (EXAFS). XANES carries mainly multi-scattering information in identifying element, chemical state, valence and coordination environment, while the relatively simple single-scattering approximation in EXAFS makes it useful to provide definitive local structure information, like bond distance and coordination numbers.[4,15,47,52] A critical review by Frenkel focusing on bimetallic catalyst structural analysis using EXAFS has been reported.[53] EXAFS spectroscopy in Chin *et al.*'s work on reduced bimetallic Au–Ni/$MgAl_2O_4$ catalysts (Fig. 6) confirmed the Au–Ni bond formation, which is distinct from those of Au–Au and Ni–Ni ones;[54] and showed increased Au–Au and decreased Au–Ni coordination numbers with increasing Au loading. It should be noted that XAS is not a surface sensitive technique. However, surface properties can dominate and XAS can be sensitive to surface structure changes when the particle sizes of

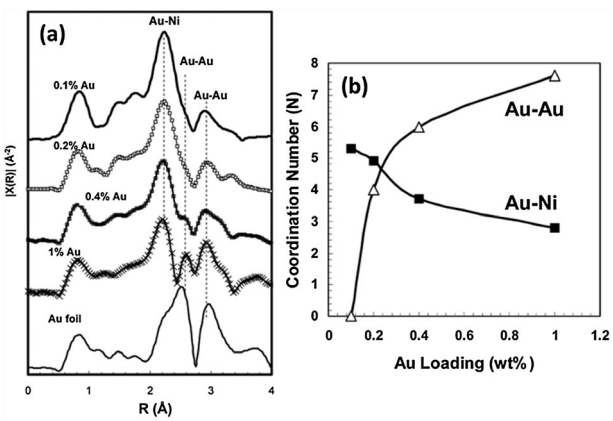

Fig. 6 (a) k^1-weighted Fourier transform of Au L_{III}-edge EXAFS for Au–8.8% Ni/$MgAl_2O_4$ after reduction at 500 °C, (b) Au–Au and Au–Ni interaction in terms of the average coordination number relationship derived from data fitting in (a).[54] Reproduced by permission of Elsevier.

studied materials (including bimetallics) are extremely small and uniform,[4] making it a useful and complementary characterization technique for NPs beyond XRD detection limit.

2.3.8 Chemisorption. Chemisorption refers to the adsorption phenomenon that involves chemical bond formation between the adsorbate molecule and the substrate (adsorbent) surface. Chemisorption provides information on catalysts' surfaces including quantitative determination of the catalytically active sites and their relative strength, metal–metal and metal–support interactions, *etc*. For bimetallic catalysts, chemisorption is widely used to measure the heat of adsorption of the probe molecules (*e.g.*, H_2, O_2, CO, CO_2). By comparing the adsorption heat on bimetallic catalysts with their monometallic counterparts, it is possible to indirectly identify the intermetallic interaction in the bimetallic catalysts. This characterization technique appears to be particularly useful and complementary to temperature-programmed desorption (TPD) and FTIR of probe molecule adsorption. Typically, a micro-calorimetric method is employed to measure the differential heat of adsorption and the heat profile as a function of the adsorbate coverage on the catalyst surface. For instance, Tanksale *et al*. reported that adding a small amount of Pt or Pd to alumina nanofiber supported Ni catalysts lowered the CO differential heat of adsorption, which was related to the Pd–Ni/Pt–Ni alloy formation corroborated by STEM/EDX.[42]

3. Bimetallic catalysts for hydrogen generation *via* reforming techniques

Reforming technique has been widely used for hydrogen production. Specifically, high-temperature steam reforming of hydrocarbons (*i.e*., methane at over 800 °C) accounts for a significant portion of commercial hydrogen generation all over the world (about 50%).[8] Another potential application of steam reforming is on-board hydrogen generation for fuel-cell powered vehicles. Various catalyst formulations including bimetallic catalysts have been reported to play key roles in improving catalyst activity and selectivity for a variety of feedstocks.

3.1 Bimetallic catalysts for steam reforming of hydrocarbons and sulfur-containing fuels

Steam reforming of hydrocarbons has been well-established in industry to produce hydrogen. This is a highly endothermic process and, in most cases, requires temperatures higher than 500 °C (800 °C for SMR). Traditional Ni catalysts suffer from severe carbon deposition at low steam/carbon (S/C) ratio (close to stoichiometry). Catalysts poisoning by inherent sulfur (up to 3000 ppm by weight) in logistic fuels remains another major challenge. Adding noble metals to Ni catalysts has been reported to increase the sulfur resistance.[55]

Recent research work on noble metal modified Ni catalysts for syngas production *via* SMR has been reviewed.[20] Li *et al*. reported that the oxidative SMR activity on Pt/Ni (SI) increased significantly compared with those on Pt + Ni (CI) and Ni.

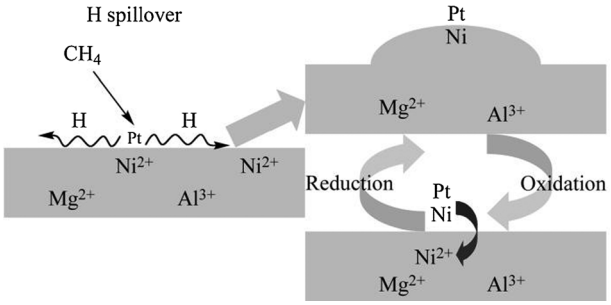

Fig. 7 A scheme of self-activation and self-regenerative activity of Pt/Ni/Mg(Al)O catalyst.[56] Note: this scheme also applies to Ru/and Rh/Ni/Mg(Al)O catalysts according to Li *et al*.[20] and references therein. Reproduced by permission of Elsevier.

TEM characterization revealed that these three catalysts have almost the same metal particle size, and the difference in reaction activity was attributed to the predominant surface Pt–Ni alloy formation on Pt/Ni (SI) (Fig. 5).[12] Other studies on trace noble metal-doped Ni/Mg(Al)O catalysts for daily start-up and shut-down (DSS) operation of SMR were carried out by the Takehira group.[20,56] A Pt-doped catalyst was reported to be most effective because of the enhanced reduction of Ni^{2+} to Ni^0 *via* hydrogen spillover from Pt or the Pt–Ni alloy. Another "intelligent" property of these noble metal doped Ni catalysts was self-regeneration, and this activity was believed to be accomplished by self-redispersion process under reaction conditions (Fig. 7). Ferrandon *et al*. found that the Ni–Rh/La–Al_2O_3 catalyst with a low Rh loading showed better performance than the monometallic Rh or Ni catalyst in steam reforming of *n*-butane; interestingly, a somewhat complicated scenario was proposed that the improved performance could be due to the co-existence of the Ni–Rh alloy, NiO_x and RhO_x.[52]

Song and co-workers studied CeO_2–Al_2O_3 (CeAl)-supported mono- and bi-metallic Ni and Rh catalysts and their tolerance to sulfur poisoning in steam reforming of hydrocarbons. Rh–Ni is believed to be the active site for hydrocarbon activation, while water molecule is activated on CeO_x.[43] At high Ni loadings, strong interaction of Rh–Ni is confirmed by TPR; Ni, as a sacrificial medium, is demonstrated to be able to protect Rh against deactivating due to sulfur poisoning.[13] The 2% Rh–10% Ni/CeAl catalyst displayed dramatic improvement in sulfur tolerance, and >95% conversion was maintained for up to 28 h time-on-stream (TOS).

3.2 Bimetallic catalysts for steam reforming of small oxygenates

Compared to hydrocarbons, steam reforming of oxygenated hydrocarbons is thermodynamically favored at relatively low temperatures.[10] In addition, small oxygenates (methanol, ethanol, acetone, acetic acid, *etc*.) are readily stored and distributed, making them ideal hydrogen carriers for on-board hydrogen generation and supply in PEMFC system. Due to its relatively low reforming temperature, ready availability, and high hydrogen content, methanol has been identified as one of the most promising ones for not only on-board but also stationary hydrogen generation.[57]

Typically, methanol steam reforming (MSR) reaction, as shown in eqn (1), is operated at 250–350 °C, 1–5 MPa with steam to methanol ratio (H_2O/CH_3OH) of 1 : 5. Early studies on this reaction focused on Cu-based catalysts which suffer from fast sintering and are pyrophoric.[8] Later, it was found that Pd/ZnO, after hydrogen pretreatment at high temperatures (> 350 °C),[28] showed a significantly lower CO selectivity than those pretreated at lower temperatures in MSR, albeit a lower activity than that of Cu-based catalysts. The preliminary results also revealed that PdZn alloy, identified by XRD, was the active phase for highly selective hydrogen production.[28] This pioneer work has since intrigued numerous investigations on the bimetallic PdZn catalysts for MSR, which have recently been reviewed.[57,58]

With more insight into the catalyst structure and reaction mechanism, it was found that particle size, morphostructure of ZnO support, and even the phase of PdZn alloy affect the activity and selectivity significantly.[58,59] With appropriate ZnO support, the Pd/ZnO catalyst could achieve an activity as high as those of Cu-based catalysts, while exhibiting much better stability in MSR.

$$CH_3OH(g) + H_2O(g) \rightarrow CO_2(g) + 3H_2(g)$$
$$\Delta H_m^{\circ}\ (298.15\ K) = 49.5\ kJ\ mol^{-1} \qquad (1)$$

Iwasa *et al.* first proposed that PdZn alloy phase was formed during reduction and altered the reaction pathway towards hydrogen and CO_2.[28] It was observed that both methanol conversion and hydrogen selectivity increased significantly with the increase of catalyst reduction temperature. The CO selectivity was below 2% on the catalyst reduced at 500 °C, close to those of Cu-based catalysts at similar reaction conditions and methanol conversions. Chin *et al.* found that a high Pd loading (*e.g.*, > 10%) is necessary to favor MSR activity and suppress CO selectivity on Pd/ZnO catalysts, which was ascribed to large-sized PdZn alloy crystallites with less defects,[29] and later confirmed by theoretical calculations.[60] Consistently, Dagle *et al.* reported that increasing reduction temperature would lead to a slight decrease in methanol conversion but more dramatic suppression on CO formation, particularly on PdZn catalysts with low Pd loadings. The suppressed CO formation was attributed to large sintered PdZn crystallites formed during high temperature reductions (650 °C) corroborated by TEM characterizations (Fig. 8c and d).[31] Similarly, Karim *et al.* also observed high CO selectivity over a catalyst populated with small crystallites (< 2 nm).[21]

Using an aerosol-derived approach, Halevi *et al.* synthesized unsupported intermetallic PdZn particles to study the specific reactivity of the alloy phase in MSR reaction.[25] A variety of X-ray and electron-based characterization techniques were used to prove that the synthesized catalyst was in a single phase with homogeneous composition. The catalyst evaluation demonstrated remarkable stability and low CO selectivity (2% at up to 270 °C). Using the same method, it was found that $PdZn_{\alpha}$ and $PdZn_{\beta 1}$ alloys were synthesized by adjusting Pd and Zn composition. $PdZn_{\beta 1}$ was identified as the active phase for low CO selectivity, while methanol decomposition leading to high CO selectivity was dominating over $PdZn_{\alpha}$ phase.[59] Very recently, Foettinger *et al.* used quick-XANES to demonstrate that PdZn alloy formation was reversibly controlled by redox cycles and a dynamic structure for the working Pd/ZnO catalyst was proposed as shown in Fig. 9.[26]

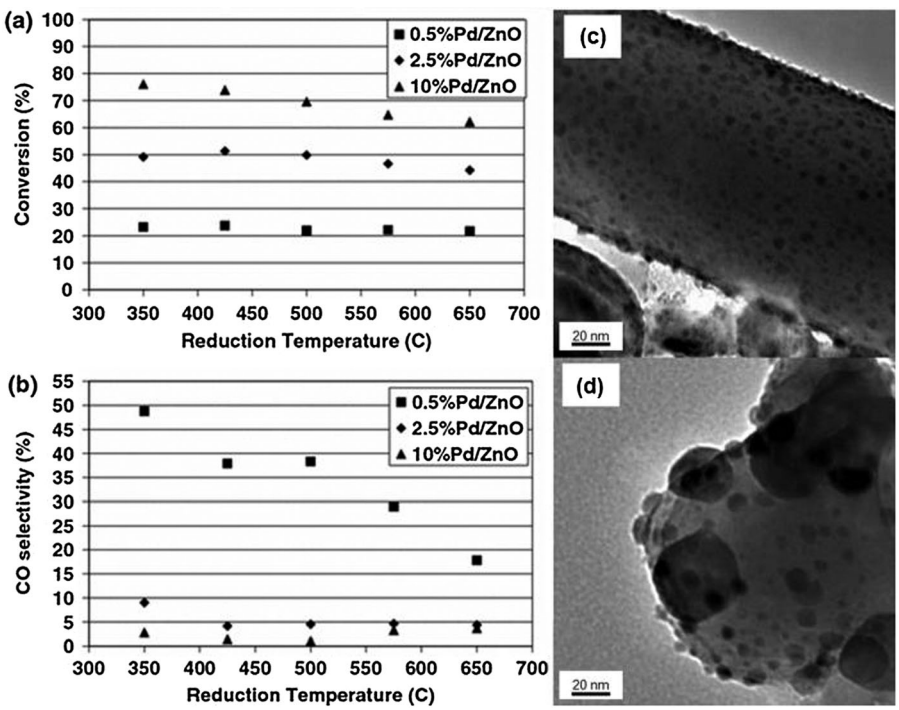

Fig. 8 (a) Conversion and (b) CO selectivity as a function of reduction temperature for Pd/ZnO catalysts (reaction temperature 275 °C), and TEM micrographs of (c) 2.5% Pd/ZnO reduced at 425 °C (average crystallite size 5.3 nm) and (d) 10% Pd/ZnO reduced at 650 °C (average crystallite size 11.4 nm).[31] Reproduced by permission of Springer.

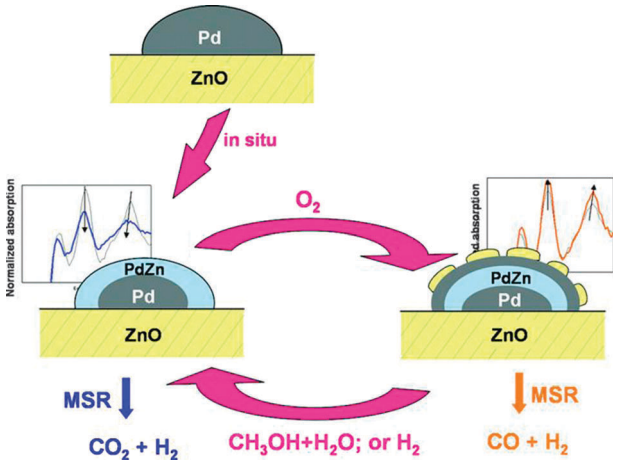

Fig. 9 Dynamic structure model of Pd/ZnO particle as MSR catalyst. *In situ* Pd K-edge XANES spectrum is shown for each structure under the corresponding reaction condition.[26] Reproduced by permission of American Chemical Society.

With respect to the role of Zn in MSR on Pd/ZnO catalyst, much work has been done but no definitive consensus appears to be reached. Study of a model single crystal catalyst by Jeroro and Vohs indicated that 25% Zn covered Pd(111) surface showed no activity toward methanol dehydrogenation.[61] However, high activity and H_2 selectivity was observed over Zn-promoted Pd on other supports (MgO, ZrO_2, CeO_2 and active carbon).[30] The distinct activity might be due to the size (NP *vs.* single crystal) and pressure (atmospheric pressure *vs.* UHV) difference in these two studies. Karim *et al.* observed a significant effect of the ZnO support morphology on MSR reactivity, and the exposed facets of ZnO appeared to play a critical role.[32] Another study of Pd on ZnO(0001) and ZnO(10$\bar{1}$0) model catalysts indicated that structure sensitivity may exist on Pd/Zn(0001) and could be attributed to synergies between Pd and the substrate as well as their interfacial sites.[46] By combining the PdZn model catalyst with spectroscopic surface analysis under UHV and reactions at realistic pressures, Rameshan *et al.* confirmed electron transfer from Zn to Pd, leading to stronger CO adsorption and longer residence time of this dehydrogenation intermediate which accounted for high CO_2 selectivity.[62]

It is worth mentioning here that bimetallic catalysis plays an important role in partial oxidation of methanol (POM) to produce hydrogen. This process is also suitable for on-board hydrogen generation for PEMFCs because of its fast reaction rates and exothermic nature which makes external heating unnecessary. Among the catalysts tested in POM, Cu- and Pd-based ones result in too much CO in the product stream which poisons the Pt electrode in PEMFCs. Recently, Au-based systems have received increasing attention due to their high selectivity to H_2. Catalyst formulations, such as Au–Ru/Fe_2O_3, Au–Cu/TiO_2 and Au–Pd/ZnO, have been proposed as possible candidates for high purity hydrogen generation.[63] However, their catalytic mechanism is still not well understood.

3.3 Bimetallic catalysts for aqueous-phase reforming

Aqueous-phase reforming (APR), as its name implies, is a reforming process conducted in aqueous phase. The application of APR in converting oxygenated hydrocarbons to H_2 and CO_2 was first reported in 2002 by Cortright *et al.*,[64] and since then, it has been developed by a number of research groups.[7,10,65] The feasibility of this technology is based on the fact that reforming of water soluble oxygenated hydrocarbons having a C : O ratio of 1 : 1 (*i.e.*, methanol (CH_3OH), ethylene glycol ($C_2H_4(OH)_2$), glycerol ($C_3H_5(OH)_3$), and sorbitol ($C_6H_8(OH)_6$), all of which can be abbreviated as $C_nH_{2n+2}O_n$ where n = 1, 2, 3 or 6) with water is thermodynamically favorable at significantly lower temperatures than those required for alkanes with similar carbon numbers, and that WGS is also more favorable at lower temperatures. Practically, APR reactions are often operated at low temperatures (200–270 °C) and medium pressures (2–5 MPa) to ensure the liquid phase operation. Compared to vapor phase reforming, the advantages of this technique include reforming of feedstocks that are difficult to vaporize without thermal degradation, relatively low energy consumption because of the unnecessity of vaporizing excess water, low CO concentration in the products due to the favorable WGS reaction, and direct generation of pressurized hydrogen under reaction condition.

The overall APR reaction is shown in eqn (2), which looks quite similar to traditional steam reforming, *e.g.*, eqn (1) when n = 1. However, under APR reaction condition methanation (eqn (3) and (4)) and Fischer–Tropsch synthesis (FTS) (eqn (5)) are thermodynamically favored, converting H_2 and CO/CO_2 to more stable side products like alkanes. Some other side reactions like dehydration/hydrogenation or dehydrogenation/rearrangement may occur to form alcohols or acids which can further react *via* decarboxylation to form alkanes.[10,65] Therefore, APR catalysts should be designed to facilitate C–C bond cleavage while mitigating C–O bond scission. Among the catalysts studied, group VIII metals are expected to exhibit high activity for breaking C–C bonds.

$$C_nH_{2n+2}O_n + nH_2O \rightarrow nCO_2 + (2n + 1)H_2 \quad (2)$$

$$CO + 3H_2 \rightarrow CH_4 + H_2O \quad (3)$$

$$CO_2 + 4H_2 \rightarrow CH_4 + 2H_2O \quad (4)$$

$$(2n + 1)H_2 + nCO \rightarrow C_nH_{2n+2} + nH_2O \quad (5)$$

Group VIII monometallic catalysts have been investigated by the Dumesic group.[10] Their kinetic data showed that the overall ethylene glycol reforming activity decreased in the order of Pt–Ni > Ru > Rh–Pd > Ir. Pt and Pd catalysts exhibited higher H_2 yield and lower alkane selectivity than other metals on silica support. Using a high-throughput reactor, Huber *et al.* screened a large number of catalysts and the results matched well with Davda's report; Ni catalysts showed the activity comparable to Pt, albeit with a lower H_2 selectivity and poorer catalyst stability.[66] Pt has been recognized as the best catalyst considering its high activity and minimized undesired C–O bond cleavage and methanation side reaction. To further improve the performances of monometallic Pt catalysts (activity, H_2 selectivity, stability) and reduce their cost, research activities have focused on bimetallic catalysts with earlier work by Huber *et al.* on Pt and Pd bimetallic catalysts for ethylene glycol APR.[66]

3.3.1 Ni–Sn. Huber *et al.* reported a Sn-doped RANEY®-Ni catalyst (R-NiSn), which showed comparable performances as the 3%Pt/Al_2O_3 catalyst for hydrogen production from ethylene glycol, glycerol, and sorbitol.[67] It was found that, compared with RANEY®-Ni, the R-NiSn catalyst showed reduced methanation rate while maintaining high C–C cleavage activity for H_2 production, and it was catalytically stable.[68] XPS, XRD and Mössbauer spectroscopy showed that Sn migrated into Ni particles to form a Ni_3Sn alloy shell around a Ni core after hydrogen reduction followed by exposure to reaction conditions. The high selectivity of R-NiSn catalysts for hydrogen production was believed to be related to either the presence of Ni_3Sn or Sn that selectively poison Ni defect or edge sites responsible for methanation of CO or CO_2.[68] Xie *et al.* also demonstrated that Sn modification drastically improved the performance (98% H_2 selectivity at 87% conversion) of Ni catalysts in ethylene glycol APR. The skeletal Ni (RQ Ni) catalyst was synthesized by impregnation of rapidly quenched $Ni_{50}Al_{50}$ alloy with $SnCl_4$ followed by thermal treatment. Catalyst characterization suggested that active sites for CO adsorption and/or dissociation significantly decreased by addition of Sn to RQ Ni, and thus the undesired methanation reaction was suppressed. In addition, the promotion of WGS reaction was attributed to facile H_2O dissociation on Sn.[33]

3.3.2 Ni–Co, Ni–Pt, Pt–Co and Pt–Mo. Luo *et al.* reported that the bimetallic Ni–Co catalyst with synergistic effect maintained good C–C bond cleavage activity and improved hydrogen selectivity.[44] Tanksale *et al.* reported an enhanced sorbitol APR performance by Pt with the alumina nanofiber (Alnf) supported bimetallic Ni–Pt catalyst.[42] H_2 formation rate on the bimetallic Ni–Pt catalyst was found to be more than five times higher than that on the Ni/Alnf catalyst. It is believed that even a very small fraction of Pt facilitated NiO reduction and therefore increased the number of active sites. A surface science study on glycerol decomposition over single crystal model catalysts by Skoplyak *et al.* revealed an increased reforming activity over Ni–Pt–Pt(111) compared to those over Pt(111) and Pt–Ni–Pt(111), in the order of Pt–Ni–Pt(111) < Pt(111) < Ni–Pt–Pt(111), which could be due to a *d* band shift closer to the Fermi level.[69]

The studies of bimetallic catalysts suggested that adding Co to Pt catalyst significantly enhanced its activity.[66] Wang *et al.* reported enhanced (three times) APR activity without affecting the selectivity on the Pt–Co catalyst supported on single-walled carbon nanotubes (SWNTs) compared to the Pt/SWNT catalyst.[15] They also hypothesized that a core–shell structure of a Co core decorated with the Pt–Co alloy as a shell could be responsible for the activity enhancement.

3.3.3 Pt–Re. Bimetallic Pt–Re catalysts have long been used for reforming processes since the introduction of Chevron's Rheniforming catalyst in 1967. Despite the numerous investigations on the correlation of catalyst structure–performance relationship, open questions still remain. The general understanding from glycerol steam reforming over this catalyst is that, during the reduction process, molecular H_2 dissociatively adsorb on Pt to form H atoms; the latter spillover to promote Re reduction to form Pt–Re bimetallic alloy NP. Due to the presence of Re, CO adsorption on neighboring Pt sites is weakened, resulting in a lower CO coverage, and thus, increased WGS rate which is mainly responsible for the increased activity compared to the monometallic Pt/C catalyst.[70] The promotion effect of a second metal to Pt in WGS reaction[41,70] will be further discussed in detail in Section 4.

King[17] and Zhang[18] *et al.* also carried out glycerol APR on Pt–Re catalysts at 225 °C and 2.93 MPa (Fig. 4c). It was found that Re addition to Pt/C significantly enhanced conversion of glycerol (more than 10 times increase in glycerol turnover frequency (TOF)). The product distribution was also changed by adding Re to Pt and the selectivity toward C_{2+} alkanes and alcohols increased, along with the production of carboxylic acids at the expense of H_2 and CO_2. NH_3-TPD (Fig. 4b) showed that the acidity generated by hydrothermal treatment was proportional to the amount of Re. *In situ* DRIFTS analysis of adsorbed pyridine suggested that the generated local surface acidity was closely associated with surface Brønsted acid site involving a Pt–Re–OH structure. Furthermore, the reaction data were correlated with the catalyst surface acidity and it was found that the ratio of dehydration to decarbonylation (C–O/C–C) increased linearly with the number of surface acid sites, indicating that surface acidity played an important role in controlling reaction pathways in the glycerol APR reactions. By comparing NH_3-TPD over Pt–Re/C and Re/C catalysts as well as the long-term stability test, allowing leaching of segregated Re in the catalyst, Zhang *et al.*[18] reported that the catalyst acidity was mainly derived from Pt–O–Re where Re was stabilized against dissolution. The active site on the Pt–Re/C catalyst was further proposed to be oxidized Pt–Re rather than the Pt–Re alloy under glycerol APR reaction conditions (Fig. 4d).

4. Au and Pt-based bimetallic catalysts for WGS

$$CO(g) + H_2O(g) \rightarrow CO_2(g) + H_2(g)$$
$$\Delta H_m^{\circ}\,(298.15\ K) = -41.2\ kJ\ mol^{-1} \qquad (6)$$

WGS is a reversible exothermic reaction in which carbon monoxide reacts with water (steam) to form carbon dioxide and hydrogen (eqn (6)). Industrial WGS process is typically conducted in two stages with efficient intermediate heat exchange in between: the first stage, also known as the high-temperature shift (HTS) step, is usually carried out at above 350 °C and 2 MPa to reduce the CO concentration in gas stream from ~10% to ~3%; the second stage, also known as the low-temperature shift (LTS) step, is often operated at about 200 °C and 2 MPa, taking advantage of the favorable WGS equilibrium to minimize the CO concentration to <0.5%. Standard industrial catalysts for the WGS process are ferrochrome (Cr_2O_3-promoted Fe_3O_4, or Fe–Cr for short) catalysts for HTS and Cu/ZnO or CoMo catalysts for LTS. Although these catalysts have been successfully applied in industrial practice, some major drawbacks still exist such as the low activity of ferrochrome catalysts at low temperatures and the sensitivity to poisoning and sintering of the Cu/ZnO catalyst. Besides, both classes of catalysts are pyrophoric and

require special activation procedure to form appropriate active phases and achieve good catalytic performances, with the Cu/ZnO catalyst being the most demanding one.[8] Additionally, a Cr-containing catalyst (*e.g.*, Fe–Cr) is not recommended for operation at low S/C ratio and none of these catalysts aforementioned give satisfactory hydrogen yield at high gas hourly space velocities (GHSV) ($>40\,000\ h^{-1}$).[71] Recent research has been focusing on Pt- and Au-based catalysts,[8] especially on Au/CeO_2. Their nonpyrophoric nature, high activity over a wide range of temperature and GHSV, as well as good stability at high temperatures due to the strong metal–support interaction render them suitable for the operations of small-scale hydrogen generation units and systems requiring fast responses such as on-board reformers for fuel cell applications.

During the past decade, the Pt–Re bimetallic catalyst has become one of the viable options for WGS process. Sato *et al.* found that adding Re to Pt/TiO_2 could improve the activity, and a combination of characterizations suggested that, in addition to surface Pt–Re bimetallic clusters, another surface compound involving both Pt (negatively charged) and Re formed during reaction. Re addition was found to strengthen CO adsorption on Pt which was believed to be the major reason for the accelerated WGS reaction.[72] Another study by Choung *et al.* indicated that the addition of Re to the $Pt/Ce_{0.46}Zr_{0.54}O_2$ catalyst also facilitated a higher Pt dispersion, and the role of Re was more complicated in enhancing the WGS activity.[73] Farrauto *et al.* tested the catalytic performance of monolith-supported Pt and Pt–Re catalysts for both LTS and HTS operations.[74] The Pt–Re catalyst showed good activity and thermal stability for HTS operation, while the Pt catalyst was found to be more suitable for LTS application. Among the research regarding novel (Au- and) Pt-based WGS catalysts, reducible metal oxide (*e.g.*, TiO_2, Fe_2O_3 or CeO_2) supports have been mainly studied because of their oxygen storage capacity and mobility, while irreducible supports (*e.g.*, SiO_2, Al_2O_3 and MgO) typically presented significantly low activity. However, a very recent study by Zhai *et al.* indicated that even on irreducible SiO_2 support, addition of a small amount of alkaline metal (sodium or potassium) could have a promotion effect on the Pt activity. It was proposed that the oxidized Pt sites were responsible for the key steps in WGS reaction and these active Pt sites could only be stabilized by certain metal cations such as Na^+, K^+ and Ce^{x+}.[75]

Over the past decade, the Flytzani-Stephanopoulos group has made extensive studies to unravel the WGS reaction mechanism on Au/CeO_2 catalysts. Early studies indicated that metallic gold or platinum NPs acted as the active phase in WGS on Pt/CeO_2 or Au/CeO_2.[76] Fu *et al.* later pointed out that nonmetallic gold or platinum species having strong interaction with surface Ce–O were the active sites, whereas the unnecessary metallic phases are only spectators.[77] Although this opinion was challenged especially with respect to the oxidation state of Au and Pt under reaction conditions,[78] there has been a general agreement that metal species in contact with oxygen vacancies on ceria are involved in the WGS reaction. Similarly, Yu *et al.* reported an enhanced WGS activity over $Au–Pt/CeO_2$ bimetallic catalysts and the primary role of Pt was believed to assist $Au^{\delta+}$ formation through charge transfer.[79]

5. Bimetallic catalysts for CO PROX in H_2-rich stream

To avoid the CO poison of anode catalysts, PEMFC requires the CO concentration in hydrogen to be maintained at trace levels (<10 ppm), and therefore a further purification step is required right after the LTS unit. Both physical and chemical routes have been used to assist this purification step, such as pressure swing adsorption (PSA), membrane separation, and CO preferential oxidation. While PSA requires high pressure operation condition and membrane separation faces the challenge of delicate membrane material with high cost, CO PROX seems to be a preferred option for its low operation temperature (<100 °C) and ready integration with PEMFC. For PROX, two parallel oxidation reactions (eqn (7) and (8)) can take place and the two products may lead to WGS and reverse WGS (RWGS) occurring simultaneously.

$$CO(g) + 0.5O_2(g) \rightarrow CO_2(g)$$
$$\Delta H_m^{\circ}\ (298.15\ K) = 283.0\ kJ\ mol^{-1} \quad (7)$$

$$H_2(g) + 0.5O_2(g) \rightarrow H_2O(g)$$
$$\Delta H_m^{\circ}\ (298.15\ K) = 241.8\ kJ\ mol^{-1} \quad (8)$$

Many catalyst formulations have been studied including metal oxides (*e.g.*, $CuO–CeO_2$) and noble metals (Au, Pt, Ru, Rh and Ir). Study on noble metal catalysts has revealed that Ru favors CO PROX. However, Ru is known to be also active for CO_2 methanation and can be readily deactivated upon exposure to oxygen-containing stream. Rh and Ir catalysts are less selective than Ru catalysts and seldom considered for this application.[80] Except the Au/Fe_2O_3 catalyst prepared *via* a special two-stage calcination process by Landon *et al.*,[81] few supported gold catalysts have shown stable activity with acceptable CO conversion. However, Au-based bimetallic catalysts are considered to enhance the overall performance.[8] Similarly, Pt catalysts also need further improvement in terms of the activity at low temperature and the efficiency on a per metal atom basis.[35]

5.1 Pt-based bimetallic catalysts

Ko *et al.* reported that an yttria-stabilized zirconia (YSZ)-supported Pt–Co bimetallic catalyst was highly active for CO PROX reaction due to the presence of isolated bimetallic Pt–Co NPs interacting with the support, and the CO concentration could be reduced to below 10 ppm.[14] Similarly, Li *et al.* reported an enhancement of PROX activity on the Al_2O_3-supported Pt–Co catalyst. Using a variety of characterization techniques, they identified the formation of Pt_3Co intermetallic particles and co-existence of Co^0 and $Co^{\delta+}$ species on the working catalyst, which was attributed to the enhanced PROX activity.[51] Ebashi *et al.* reported that Re modification had a promoting effect depending on the Re oxidation state.[16] Xu *et al.* studied both the Fe–Pt(111) single crystal model catalyst and particle supported Pt–Fe NPs, and showed the co-existence of Fe ensemble and surface PtFe alloy.[82] It was found that Fe ensemble was active and stable in PROX reaction but became inactive in CO oxidation in the absence of H_2 due to the full oxidation of the metal surface, whereas the PtFe alloy remained

stable in both reactions. Nilekar *et al*. synthesized a series of catalysts with transition metal cores (M = Ru, Rh, Ir, Pd and Au) and Pt shell, and found that the PROX activity in terms of the core metal decreased in the order of Ru > Rh > Ir > Pd > Au.[23] The reactivity was found to have a strong relationship with the influence of the metal core on the CO binding energy on the Pt shell which could further affect the CO saturation coverage. Zhang *et al*. showed that Pd–Pt alloy nanocages supported on ZnO nanowires enhanced activity and selectivity for the PROX reaction compared with the parent monometallic Pd nanocube and commercial Pt/C catalysts.[24] Schubert *et al*. confirmed a much lower activation energy for PROX reaction over Pt_3Sn/C than that over the Pt/Al_2O_3 catalyst and proposed that Pt sites were mainly responsible for CO or H_2 adsorption while Sn and SnO_x for O_2 adsorption.[45] Kuriyama *et al*. reported that potassium addition to Pt/Al_2O_3 enhanced the PROX activity, and attributed such an enhancement to a weaker interaction between CO and Pt, and the altered CO adsorption site was corroborated by *in situ* FTIR characterization.[83]

5.2 Au-based bimetallic catalysts

Au has also been suggested as a potential low temperature PROX catalyst. Recent research on Au-based bimetallic PROX catalysts has shown that Cu is a good candidate as the second metal species due to its inherent PROX activity and structural similarity with Au. Liu *et al*. reported a synergistic effect on bimetallic $Au–Cu/SiO_2$ catalysts to account for the superior performance to the monometallic Au catalyst.[34]

Table 2 Summary of bimetallic catalysts for hydrogen production

Process	Catalyst	Method of preparation	Performance	Active species	Note & Ref.
Oxidative SMR	Pt–Ni/ γ-Al_2O_3	SI and CI	Activity: Pt/Ni (SI) ~ Pt + Ni (CI) > Ni	Surface Pt–Ni alloy	Pt inhibits Ni oxidation[12]
Steam reforming of *n*-butane	Ni–Rh/ La–Al_2O_3	CI	Activity: Ni–Rh > Rh > Ni	Co-existence of Ni–Rh alloy, NiO_x and RhO_x	No coke formation over Ni–Rh/$CeZrO_2$[52]
Steam reforming of jet fuel	2% Rh–10% Ni/CeO_2–Al_2O_3	CI	Activity: > 97% conversion, sulfur tolerant over Rh–Ni bimetallic catalyst	Rh–Ni site	>95% conversion over 3 days for JP-8 jet fuel containing 22 ppm sulfur[13]
MSR	Pd/ZnO	IWI	Complete conversion below 300 °C with CO selectivity < 4%;	Pd–Zn alloy particle	Moderate reaction temperature and mild reducing condition;[29] bigger PdZn particles suppress CO formation;[21,31]
	PdZn alloy powder	Aerosol-derived approach	TOF: PdZn ≫ Pd; CO selectivity < 2% over $PdZn_{\beta 1}$	Pd–Zn alloy ($PdZn_{\beta 1}$ and $PdZn_{\alpha}$ phases)	$PdZn_{\beta 1}$ phase is critical for low CO selectivity[59]
POM	Au–Ru/Fe_2O_3, Au–Cu/TiO_2	DP	Generally higher conversion than that over monometallic Au catalysts, some with 100% H_2 selectivity	Bimetallic alloy	Not well understood catalytic mechanism[63]
APR of $C_nH_{2n+2}O_n$ (n = 2, 3, 6)	RANEY® Ni–Sn	Impregnation followed by hydrothermal treatment	Comparable with Pt/Al_2O_3	Ni–Sn alloy surface	Sn addition greatly suppresses methane formation[67]
APR of ethylene glycol	Skeleton $Ni_{80}Sn_{20}$	Impregnation	98% H_2 selectivity at above 87% conversion	Bifunctional Ni–Sn ensemble	WGS is promoted *via* H_2O dissociation on Sn and CO adsorption on Ni[33]
	Pt–Co/SWNT	SI	Three-fold conversion compared with Pt/SWNT	Close contact of Pt and Co species	Core–shell structure on the catalyst surface-Co core decorated with Pt–Co alloy[15]
APR of glycerol	3% Pt–3% Re/C	SI	> ten times TOF enhancement compared with 3% Pt/C	Oxidized Pt–Re	Surface acidity facilitates dehydration pathway[18]
WGS	Au–Pt/CeO_2	SI	Four times (220 °C) and nearly two times (250 °C) conversion compared to Au/CeO_2	Ionic gold species interacting with Pt through charge transfer and Ce^{3+} through oxygen bonding	The particle size and structure of CeO_2 support are also affected by the metal loading which contributes to the overall performance improvement[79]
CO PROX	Pt–Co/YSZ	CI	Significant improvement of activity compared with Pt/YSZ	Pt–Co NP interacting with support	Calcination and reduction temperature have a great impact on the bimetallic structure[14]
	M@Pt core–shell NP (M = Ru, Rh, Ir, Pd, Au)	Liquid-phase synthesis	Activity decreasing in the order of: Ru > Rh > Ir > Pd > Au	M@Pt core–shell NP	Two scenarios are proposed for the difference in PROX activity: (i) relative availability of CO-free Pt site, (2) H_2-mediated low-temperature CO oxidation
	Au–Cu/SiO_2	Modified DP	Au–Cu/SiO_2 exhibiting superior performance to Au/SiO_2 or Cu/SiO_2	Au–Cu alloy NP	Decreasing CO conversion and CO_2 selectivity with increasing Au/Cu ratio (no activity over Cu/SiO_2) was observed[34]

Fonseca *et al.* found that, for monometallic catalysts, Au/CeO_2 was much more active than Cu/CeO_2, while its selectivity was lower; the Au–Cu bimetallic catalyst was reported to exhibit an intermediary behavior.[84] Despite the observed performance differences, insightful catalyst characterization has been scarcely reported to differentiate the structural information and other properties on the bi- and mono-metallic catalysts. Li *et al.* found that Au–Cu/SBA-15 exhibited extremely high activity at room temperature; however, fast deactivation was also observed.[85] Based on the experimental evidences, the authors proposed that a combination of reversible redox cycle, Cu migration and Au–Cu alloy/dealloy took place during the catalyst activation–deactivation process and the Au–Cu alloy formation was the main reason for catalyst deactivation which can be reversed *via* a simple calcination step to restore the catalyst activity.

6. Conclusion

Catalytic steam reforming serves as one of the most important techniques for hydrogen production. Although high-temperature SMR has been widely practiced for large-scale hydrogen production and accounts for the majority of current hydrogen supply, developing low-temperature and highly efficient reforming technologies for on-board hydrogen production for fuel cells still remains challenging. We have reviewed recent progresses and important contributions to bimetallic catalysts for hydrogen production as well as the down-stream purification processes. By applying appropriate bimetallic catalysts, enhanced catalytic performances can be achieved compared to the monometallic counterpart. A summary of bimetallic catalyst application for hydrogen production can be found in Table 2. It was demonstrated that catalyst synthesis and treatment usually play key roles in affecting the bimetallic catalyst structure and properties which subsequently influence their catalytic behaviors. The enhancement in catalytic performance of bimetallic catalysts is generally attributed to the intimate interaction between two metals. Development of new synthesis methods will enable the control of particle size, shape, composition and stability of bimetallic catalysts. Advanced catalyst characterizations can provide insights into the chemical and structural information on bimetallic catalysts which helps unravel the mechanisms and reaction pathways. The advancement of *in situ* characterization, especially with the possibility of monitoring the catalyst surface under realistic conditions,[86–88] provides fundamental understanding of structure–activity relationship of bimetallic catalysts in hydrogen production, which in turn can guide the design of improved catalysts for low temperature on-board hydrogen production.

7. Abbreviations

APR	Aqueous-phase reforming
APXPS	Ambient-pressure X-ray photoelectron spectroscopy
ATR-IRS	Attenuated total reflectance infrared spectroscopy
CI	Co-impregnation
CP	Co-precipitation
DP	Deposition-precipitation
DRIFTS	Diffuse reflectance infrared Fourier transform spectroscopy
EDX	Energy-dispersive X-ray spectroscopy
EXAFS	Extended X-ray absorption fine structure
FTIR	Fourier transform infrared spectroscopy
FTS	Fischer–Tropsch synthesis
GHSV	Gas hourly space velocity
HAADF-STEM	High angle annular dark field scanning transmission electron microscope
HRTEM	High-resolution transmission electron microscope
HTS	High-temperature shift
IWI	Incipient wetness impregnation
LTS	Low-temperature shift
MSR	Methanol steam reforming
NP	Nanoparticle
PEMFC	Proton exchange membrane fuel cell
POM	Partial oxidation of methanol
PROX	Preferential oxidation
PSA	Pressure swing adsorption
S/C	Steam to carbon ratio
SEM	Scanning electron microscopy
SI	Sequential impregnation
SMR	Steam methane reforming
STM	Scanning tunneling microscopy
SWNT	Single-walled carbon nanotube
TOF	Turnover frequency
TPD/R	Temperature-programmed desorption/reduction
WGS	Water-gas shift
XANES	X-ray absorption near-edge structure
XAS	X-ray absorption spectroscopy
XPS	X-ray photoelectron spectroscopy
XRD	X-ray diffraction
YSZ	Yttria-stabilized zirconia

Acknowledgements

We acknowledge the financial support from the US Department of Energy (DOE), Office of Basic Energy Sciences, Division of Chemical Sciences, Geosciences, and Biosciences.

References

1 N. Toshima and T. Yonezawa, *New J. Chem.*, 1998, **22**, 1179–1201.
2 J. H. Sinfelt, *Bimetallic catalysts: Discoveries, concepts, and applications*, Wiley, New York, 1983.
3 C. J. Liu, U. Burghaus, F. Besenbacher and Z. L. Wang, *ACS Nano*, 2010, **4**, 5517–5526.
4 O. S. Alexeev and B. C. Gates, *Ind. Eng. Chem. Res.*, 2003, **42**, 1571–1587.
5 D. S. Wang and Y. D. Li, *Adv. Mater.*, 2011, **23**, 1044–1060.
6 J. G. Chen, C. A. Menning and M. B. Zellner, *Surf. Sci. Rep.*, 2008, **63**, 201–254.
7 J. D. Holladay, J. Hu, D. L. King and Y. Wang, *Catal. Today*, 2009, **139**, 244–260.
8 K. Liu, C. S. Song and V. Subramani, *Hydrogen and syngas production and purification technologies*, Wiley, Hoboken, NJ, 2010.
9 J. N. Armor, *Appl. Catal., A*, 1999, **176**, 159–176.
10 R. R. Davda, J. W. Shabaker, G. W. Huber, R. D. Cortright and J. A. Dumesic, *Appl. Catal., B*, 2005, **56**, 171–186.
11 Y. H. Chin, Y. Wang, R. A. Dagle and X. H. S. Li, *Fuel Process. Technol.*, 2003, **83**, 193–201.

12 B. Li, S. Kado, Y. Mukainakano, T. Miyazawa, T. Miyao, S. Naito, K. Okumura, K. Kunimori and K. Tomishige, *J. Catal.*, 2007, **245**, 144–155.
13 J. J. Strohm, J. Zheng and C. S. Song, *J. Catal.*, 2006, **238**, 309–320.
14 E. Y. Ko, E. D. Park, H. C. Lee, D. Lee and S. Kim, *Angew. Chem., Int. Ed.*, 2007, **46**, 734–737.
15 X. M. Wang, N. Li, L. D. Pfefferle and G. L. Haller, *Catal. Today*, 2009, **146**, 160–165.
16 T. Ebashi, Y. Ishida, Y. Nakagawa, S. Ito, T. Kubota and K. Tomishige, *J. Phys. Chem. C*, 2010, **114**, 6518–6526.
17 D. L. King, L. A. Zhang, G. Xia, A. M. Karim, D. J. Heldebrant, X. Q. Wang, T. Peterson and Y. Wang, *Appl. Catal., B*, 2010, **99**, 206–213.
18 L. Zhang, A. M. Karim, M. H. Engelhard, Z. Wei, D. L. King and Y. Wang, *J. Catal.*, 2012, **287**, 37–43.
19 J. M. Sun and X. H. Bao, *Chem.–Eur. J.*, 2008, **14**, 7478–7488.
20 D. Li, Y. Nakagawa and K. Tomishige, *Appl. Catal., A*, 2011, **408**, 1–24.
21 A. Karim, T. Conant and A. Datye, *J. Catal.*, 2006, **243**, 420–427.
22 J. R. Regalbuto, *Catalyst preparation: Science and engineering*, CRC Press/Taylor & Francis Group, LLC, Boca Raton, FL, 2007.
23 A. U. Nilekar, S. Alayoglu, B. Eichhorn and M. Mavrikakis, *J. Am. Chem. Soc.*, 2010, **132**, 7418–7428.
24 H. Zhang, M. S. Jin, H. Y. Liu, J. G. Wang, M. J. Kim, D. R. Yang, Z. X. Xie, J. Y. Liu and Y. N. Xia, *ACS Nano*, 2011, **5**, 8212–8222.
25 B. Halevi, E. J. Peterson, A. DeLaRiva, E. Jeroro, V. M. Lebarbier, Y. Wang, J. M. Vohs, B. Kiefer, E. Kunkes, M. Havecker, M. Behrens, R. Sehloegl and A. K. Datye, *J. Phys. Chem. C*, 2010, **114**, 17181–17190.
26 K. Foettinger, J. A. van Bokhoven, M. Nachtegaal and G. Rupprechter, *J. Phys. Chem. Lett.*, 2011, **2**, 428–433.
27 B. M. Weckhuysen, *Chem. Soc. Rev.*, 2010, **39**, 4557–4559.
28 N. Iwasa, S. Masuda, N. Ogawa and N. Takezawa, *Appl. Catal., A*, 1995, **125**, 145–157.
29 Y. H. Chin, R. Dagle, J. L. Hu, A. C. Dohnalkova and Y. Wang, *Catal. Today*, 2002, **77**, 79–88.
30 N. Iwasa, T. Mayanagi, W. Nomura, M. Arai and N. Takezawa, *Appl. Catal., A*, 2003, **248**, 153–160.
31 R. A. Dagle, Y.-H. Chin and Y. Wang, *Top. Catal.*, 2007, **46**, 358–362.
32 A. M. Karim, T. Conant and A. K. Datye, *Phys. Chem. Chem. Phys.*, 2008, **10**, 5584–5590.
33 F. Z. Xie, X. W. Chu, H. R. Hu, M. H. Qiao, S. R. Yan, Y. L. Zhu, H. Y. He, K. N. Fan, H. X. Li, B. N. Zong and X. X. Zhang, *J. Catal.*, 2006, **241**, 211–220.
34 X. Y. Liu, A. Q. Wang, T. Zhang, D. S. Su and C. Y. Mou, *Catal. Today*, 2011, **160**, 103–108.
35 B. Qiao, A. Wang, X. Yang, L. F. Allard, Z. Jiang, Y. Cui, J. Liu, J. Li and T. Zhang, *Nat. Chem.*, 2011, **3**, 634–641.
36 F. Tao, D. Tang, M. Salmeron and G. A. Somorjai, *Rev. Sci. Instrum.*, 2008, **79**, 084101.
37 S. R. Longwitz, J. Schnadt, E. K. Vestergaard, R. T. Vang, I. Stensgaard, H. Brune and F. Besenbacher, *J. Phys. Chem. B*, 2004, **108**, 14497–14502.
38 F. Tao, S. Dag, L.-W. Wang, Z. Liu, D. R. Butcher, H. Bluhm, M. Salmeron and G. A. Somorjai, *Science*, 2010, **327**, 850–853.
39 G. A. Somorjai and C. J. Kliewer, *React. Kinet. Catal. Lett.*, 2009, **96**, 191–208.
40 S. Monyanon, S. Pongstabodee and A. Luengnaruemitchai, *J. Power Sources*, 2006, **163**, 547–554.
41 D. A. Simonetti, E. L. Kunkes and J. A. Dumesic, *J. Catal.*, 2007, **247**, 298–306.
42 A. Tanksale, J. N. Beltramini, J. A. Dumesic and G. Q. Lu, *J. Catal.*, 2008, **258**, 366–377.
43 Y. Li, X. X. Wang, C. Xie and C. S. Song, *Appl. Catal., A*, 2009, **357**, 213–222.
44 N. J. Luo, K. Ouyang, F. H. Cao and T. C. Xiao, *Biomass Bioenergy*, 2010, **34**, 489–495.
45 M. M. Schubert, M. J. Kahlich, G. Feldmeyer, M. Huttner, S. Hackenberg, H. A. Gasteiger and R. J. Behm, *Phys. Chem. Chem. Phys.*, 2001, **3**, 1123–1131.
46 M. P. Hyman, V. M. Lebarbier, Y. Wang, A. K. Datye and J. A. Vohs, *J. Phys. Chem. C*, 2009, **113**, 7251–7259.
47 P. Dietrich, R. Lobo-Lapidus, T. Wu, A. Sumer, M. Akatay, B. Fingland, N. Guo, J. Dumesic, C. Marshall, E. Stach, J. Jellinek, W. Delgass, F. Ribeiro and J. Miller, *Top. Catal.*, 2012, **55**, 53–69.
48 D. F. Ogletree, H. Bluhm, G. Lebedev, C. S. Fadley, Z. Hussain and M. Salmeron, *Rev. Sci. Instrum.*, 2002, **73**, 3872–3877.
49 F. Tao, M. E. Grass, Y. Zhang, D. R. Butcher, J. R. Renzas, Z. Liu, J. Y. Chung, B. S. Mun, M. Salmeron and G. A. Somorjai, *Science*, 2008, **322**, 932–934.
50 J.-M. Andanson and A. Baiker, *Chem. Soc. Rev.*, 2010, **39**, 4571–4584.
51 H. L. Li, X. H. Yu, S. T. Tu, J. Y. Yan and Z. D. Wang, *Appl. Catal., A*, 2010, **387**, 215–223.
52 M. Ferrandon, A. J. Kropf and T. Krause, *Appl. Catal., A*, 2010, **379**, 121–128.
53 A. I. Frenkel, *Chem. Soc. Rev*, 2012, DOI: 10.1039/c2cs35174a.
54 Y. H. Chin, D. L. King, H. S. Roh, Y. Wang and S. M. Heald, *J. Catal.*, 2006, **244**, 153–162.
55 C. Hulteberg, *Int. J. Hydrogen Energy*, 2012, **37**, 3978–3992.
56 K. Takehira, *J. Nat. Gas Chem.*, 2009, **18**, 237–259.
57 D. R. Palo, R. A. Dagle and J. D. Holladay, *Chem. Rev.*, 2007, **107**, 3992–4021.
58 S. Sa, H. Silva, L. Brandao, J. M. Sousa and A. Mendes, *Appl. Catal., B*, 2010, **99**, 43–57.
59 B. Halevi, E. J. Peterson, A. Roy, A. DeLariva, E. Jeroro, F. Gao, Y. Wang, J. M. Vohs, B. Kiefer, E. Kunkes, M. Hävecker, M. Behrens, R. Schlögl and A. K. Datye, *J. Catal.*, 2012, **291**, 44–54.
60 K. H. Lim, Z. X. Chen, K. M. Neyman and N. Rosch, *J. Phys. Chem. B*, 2006, **110**, 14890–14897.
61 E. Jeroro and J. M. Vohs, *J. Am. Chem. Soc.*, 2008, **130**, 10199–10207.
62 C. Rameshan, W. Stadlmayr, C. Weilach, S. Penner, H. Lorenz, M. Hävecker, R. Blume, T. Rocha, D. Teschner, A. Knop-Gericke, R. Schlögl, N. Memmel, D. Zemlyanov, G. Rupprechter and B. Klötzer, *Angew. Chem., Int. Ed.*, 2010, **49**, 3224–3227.
63 K. L. Hohn and Y. C. Lin, *ChemSusChem*, 2009, **2**, 927–940.
64 R. D. Cortright, R. R. Davda and J. A. Dumesic, *Nature*, 2002, **418**, 964–967.
65 A. Tanksale, J. N. Beltramini and G. M. Lu, *Renewable Sustainable Energy Rev.*, 2010, **14**, 166–182.
66 G. W. Huber, J. W. Shabaker, S. T. Evans and J. A. Dumesic, *Appl. Catal., B*, 2006, **62**, 226–235.
67 G. W. Huber, J. W. Shabaker and J. A. Dumesic, *Science*, 2003, **300**, 2075–2077.
68 J. W. Shabaker, G. W. Huber and J. A. Dumesic, *J. Catal.*, 2004, **222**, 180–191.
69 O. Skoplyak, M. A. Barteau and J. G. Chen, *ChemSusChem*, 2008, **1**, 524–526.
70 E. L. Kunkes, D. A. Simonetti, J. A. Dumesic, W. D. Pyrz, L. E. Murillo, J. G. G. Chen and D. J. Buttrey, *J. Catal.*, 2008, **260**, 164–177.
71 C. Ratnasamy and J. P. Wagner, *Catal. Rev.: Sci. Eng.*, 2009, **51**, 325–440.
72 Y. Sato, K. Terada, S. Hasegawa, T. Miyao and S. Naito, *Appl. Catal., A*, 2005, **296**, 80–89.
73 S. Y. Choung, M. Ferrandon and T. Krause, *Catal. Today*, 2005, **99**, 257–262.
74 R. J. Farrauto, Y. Liu, W. Ruettinger, O. Ilinich, L. Shore and T. Giroux, *Catal. Rev.: Sci. Eng.*, 2007, **49**, 141–196.
75 Y. P. Zhai, D. Pierre, R. Si, W. L. Deng, P. Ferrin, A. U. Nilekar, G. W. Peng, J. A. Herron, D. C. Bell, H. Saltsburg, M. Mavrikakis and M. Flytzani-Stephanopoulos, *Science*, 2010, **329**, 1633–1636.
76 A. Trovarelli, *Catal. Rev.: Sci. Eng.*, 1996, **38**, 439–520.
77 Q. Fu, H. Saltsburg and M. Flytzani-Stephanopoulos, *Science*, 2003, **301**, 935–938.
78 J. A. Rodriguez, *Catal. Today*, 2011, **160**, 3–10.
79 Q. Yu, W. Chen, Y. Li, M. Jin and Z. Suo, *Catal. Today*, 2010, **158**, 324–328.
80 E. D. Park, D. Lee and H. C. Lee, *Catal. Today*, 2009, **139**, 280–290.
81 P. Landon, J. Ferguson, B. E. Solsona, T. Garcia, A. F. Carley, A. A. Herzing, C. J. Kiely, S. E. Golunski and G. J. Hutchings, *Chem. Commun.*, 2005, 3385–3387.

82 H. Xu, Q. Fu, Y. X. Yao and X. H. Bao, *Energy Environ. Sci.*, 2012, **5**, 6313–6320.
83 M. Kuriyama, H. Tanaka, S.-i. Ito, T. Kubota, T. Miyao, S. Naito, K. Tomishige and K. Kunimori, *J. Catal.*, 2007, **252**, 39–48.
84 J. d. S. L. Fonseca, H. S. Ferreira, N. Bion, L. Pirault-Roy, M. d. C. Rangel, D. Duprez and F. Epron, *Catal. Today*, 2012, **180**, 34–41.
85 X. Li, S. S. S. Fang, J. Teo, Y. L. Foo, A. Borgna, M. Lin and Z. Zhong, *ACS Catal.*, 2012, 360–369.
86 F. Tao, M. E. Grass, Y. Zhang, D. R. Butcher, F. Aksoy, S. Aloni, V. Altoe, S. Alayoglu, J. R. Renzas, C.-K. Tsung, Z. Zhu, Z. Liu, M. Salmeron and G. A. Somorjai, *J. Am. Chem. Soc.*, 2010, **132**, 8697–8703.
87 F. Tao and M. Salmeron, *Science*, 2011, **331**, 171–174.
88 F. Zaera, *Chem. Rev.*, 2012, **112**, 2920–2986.

